A RAIRS, TPD and femtosecond laser-induced desorption study of CO, NO and coadsorbed CO + NO on Pd(111)

Jadranka Butorac[1], Emma L. Wilson[1], Helen H. Fielding[1], Wendy A. Brown[1,3] and Russell S. Minns[*1,2]

[1]*Department of Chemistry, University College London, 20 Gordon Street, London WC1H 0AJ, UK*

[2]*Chemistry, University of Southampton, Highfield, Southampton SO17 1BJ, UK*

[3]*Division of Chemistry, University of Sussex, Falmer, Brighton BN1 9QJ, UK*

Abstract

Here we present a systematic study of the adsorption and laser induced desorption of CO, NO and CO + NO from a Pd(111) surface at a number of different coverages. We begin by characterising the surfaces using reflection-absorption infrared spectroscopy (RAIRS) and temperature-programmed desorption (TPD). Experiments show that NO displaces pre-adsorbed CO considerably, but that CO has a much smaller effect on pre-adsorbed NO. In both cases, the preferred binding sites of CO are occupied by NO, displacing it to less favourable adsorption sites. Femtosecond laser induced desorption (fs-LID) shows that desorption of CO on Pd(111) follows a power law and is fairly independent of CO coverage, but for NO on Pd(111) we observe a clear deviation from a power law curve at higher coverages, with saturation being observed. This suggests that the cross-section for LID of NO is much larger than that for CO and that NO on Pd(111) is more photoactive than CO on Pd(111). Interestingly, for CO + NO on Pd(111) we find that coadsorption has a strong influence on the photodesorption process and that the structure of the overlayer is also important in controlling the photodesorption products, regardless of the order in which the two molecules are dosed.

1. Introduction

The adsorption of molecules on transition metal surfaces is the primary step in the heterogeneous catalysis of a large number of technologically important processes. Hence, understanding the adsorption and subsequent desorption of the relevant species has been a primary goal of surface science for many years. More recently, new techniques based on ultrafast laser induced desorption have opened a window into the dynamics of these processes,[1-17] potentially providing new routes to photoinduced chemical activity.[18-19] Of particular relevance to the work presented here are the fundamental catalytic reactions of CO and NO on Pd(111). Coadsorbed CO and NO on Pd(111) have been studied previously using reflection absorption infrared spectroscopy (RAIRS) and temperature programmed desorption

(TPD) at a range of temperatures and pressures.[20] These measurements provide detailed information on the overlayer structure. However, very little information about the reactions of the coadsorbed CO and NO on this surface has been determined. In RAIRS experiments at high temperature (500 K) and pressure (0.1 mbar), a band observed at ~2240 cm^{-1} was assigned to the formation of NCO, which was the only product observed.[20] TPD measurements of coadsorbed CO and NO on Pd(111) showed the formation of the associative desorption product N_2.[20] To the best of our knowledge there have been no other reports of reactive products following the coadsorption of CO and NO on Pd(111) in either low or high pressure experiments.

Studies of molecular adsorbate systems using femtosecond lasers allow us to gain insight into the mechanism of the desorption process that cannot be achieved using conventional surface science techniques. The first femtosecond laser desorption study by Prybla *et al*[5] reported a non-linear rise in the desorption yield of NO on Pd(111) as a function of laser fluence. These experiments also measured the vibrational energy distribution of the desorbed molecule and found that this was much higher than in the thermal desorption process. The difference between these measurements and those derived from more conventional desorption experiments arises from the non-equilibrium temperature profile that femtosecond excitation produces. The laser pulse energy is deposited into the metal surface, leading to a rapid heating of the electrons up to temperatures of several thousand Kelvin. The hot electrons then thermalise rapidly and couple to the phonons, as well as to the adsorbate. After about a picosecond, the electron and phonon temperatures equilibrate. However, in the short time before this there can be a large difference between the two temperatures.[21] The different temperature of the electrons and phonons means that the desorption of an adsorbate driven by an electron mediated process will experience a very different temperature profile to that driven by a phonon mediated process, providing an opportunity to derive the mechanism driving a particular desorption reaction. With more conventional techniques, the temperature remains in equilibrium throughout the experiment meaning that the separation of electron and phonon mediated mechanisms is often difficult.

Since the initial measurement of NO on Pd(111),[5] a number of other systems have been studied using femtosecond laser induced desorption (fs-LID) which show similar non-linear rises in the desorption yield as a function of laser fluence,[1-16] as well as those that exhibit associative desorption[17] and other chemical reactions[22]. While a number of molecular systems have been investigated, to the best of our knowledge no coadsorbed systems have been previously studied in this way. In this article, we describe a series of experiments

investigating CO and NO individually, and coadsorbed on a Pd(111) surface using a combination of RAIRS, TPD and fs-LID. In particular, we use the different techniques to investigate the effect of coadsorption of CO and NO and the reaction products that are observed as a result of this coadsorption.

2. Methods

The ultra-high vacuum (UHV) chamber used for these experiments has two experimental levels: an upper level containing a quadrupole mass spectrometer (QMS) for TPD and fs-LID experiments, and a lower level for surface cleaning and characterisation by low-energy electron diffraction (LEED) and RAIRS. All gases were dosed via a high precision leak valve with the sample Pd(111) held at approximately room temperature. CO and NO were dosed in gaseous form and isotopic ^{13}CO and ^{15}NO were used in coadsorption experiments to allow us to distinguish reaction products with similar masses in TPD experiments. In all cases, isotope effects were tested for and were not observed. Mass spectrometer signals were corrected for the different sensitivity to different isotopes, allowing a direct comparison between TPD spectra recorded for the different isotopes.

RAIR spectra were recorded using a Thermo Nicolet 6700 Fourier-transform infrared (FTIR) spectrometer with a liquid nitrogen cooled mercury cadmium telluride (MCT) detector. Reported RAIR spectra are recorded as the sum of 256 scans with a resolution of 4 cm^{-1}. TPD and fs-LID experiments employed a Hiden pulsed ion counting QMS. The heating rate for all TPD experiments was 0.5 K s^{-1}. For all experiments involving the mass spectrometer, the Pd(111) sample face was normal to the entrance of the QMS to maximise the signal entering the QMS. This requires the angle of incidence of the laser on the sample to be 45°. A schematic of the experimental layout is presented in Figure 1.

The femtosecond laser system comprises an ultrafast oscillator (Coherent Micra) and amplifier (Coherent Legend) producing 2.5 mJ pulses at 800 nm with a pulse duration of approximately 40 fs. For the experiments described in this paper, the laser is operated at 20 Hz and is synchronised with the QMS. The fluence at the sample could be controlled continuously from 0-35 mJ cm^{-2} using a half-waveplate and polarising beamsplitter. For each experiment, the laser spot size at the sample was controlled using a telescope to reduce the beam diameter to approximately 1 mm. The exact diameter was determined from knife edge and beam profile camera measurements, allowing the calculation of the yield weighted fluence,[11] for each set of measurements. The fluence is corrected to account for reflection

losses from the sample using the Fresnel equations[23] and corresponds to the absorbed fluence assuming that all light that is not reflected is absorbed by the surface.

For all experiments, the Pd(111) surface was cleaned before exposure to CO or NO. Cleaning consisted of two cycles of 1 kV Ar^+ sputtering, annealing to 1200 K and cooling from 800 K – 500 K in oxygen to allow chemical cleaning by adsorbed O atoms. A final cycle of Ar^+ sputtering was then undertaken. Surface cleanliness and order was confirmed by LEED. Surface coverages were characterised *via* RAIRS and TPD (see Results) to ensure that fs-LID experiments were being performed on well characterised surfaces. After dosing, residual CO or NO were pumped away and their levels were measured using the QMS for 1 minute, to provide a background level and to ensure equilibrium conditions. The sample was then exposed to a series of laser pulses and the desorption yield for each laser shot was measured using the QMS. After approximately 200 laser shots, no further change in desorption was observed. The laser beam was then blocked, the sample was translated to a new position and another set of desorption measurements was recorded. Each set of desorption measurements produced a decay curve showing a reduction in the number of desorbed molecules with each laser pulse. To quantify the desorption, the first shot desorption yield was determined. A biexponential decay curve was fitted to the experimental data, providing a value for the first shot desorption yield (Figure 1). Although we collect data until the desorption from the surface does not change with subsequent laser pulses, we do not convert the desorption yield to monolayers (ML) due to diffusion of molecules on the surface into the interaction area preventing the desorption yield returning to its true baseline value. The size of the sample permits 5 data sets to be collected before cleaning and re-dosing the sample. Between measurements, cleaning by thermal desorption proved sufficient for the CO doped sample; however for experiments involving NO, a full cleaning process was required due to dissociation of NO generating strongly bound atomic oxygen.

Yield *versus* fluence measurements were obtained using the procedure outlined above for CO and NO exposures of 2, 4 and 10 L (where 1 Langmuir, L = 10^{-6} Torr s) and laser fluences between 0 and 350 J m^{-2}. To analyse the data, the points were fitted to a power law of the form

$$Y_{FS} \, \alpha \, \langle F \rangle^b, \qquad (1)$$

where Y_{FS} is the desorption yield in counts s^{-1}, $\langle F \rangle$ is the yield weighted fluence in J m^{-2} and b is a variable in the fitting procedure whose magnitude is related to the coupling strength and

desorption energy. The choice of function is empirical and follows the procedure used by other groups.[5,14,16]

3. Results and Discussion

3.1 Overlayer characterisation

In order to analyse the fs-LID data the coverage and bonding of the individual CO and NO species on the Pd(111) surface must be characterised. To monitor the changes in surface coverage, bonding site and binding strengths, RAIRS and TPD experiments were performed for CO on Pd(111), NO on Pd(111) and for a Pd(111) surface dosed with coadsorbed CO and NO. This analysis is performed for surfaces that are initially dosed with either CO or NO to ascertain if the order of adsorption is significant. For the remainder of the paper, for coadsorbed NO + CO, we will refer to the surfaces as *secondary dosed molecule/primary dosed molecule/surface* e.g. 4 L NO/ 2 L CO/ Pd(111) implies that 2 L CO was initially dosed onto a Pd(111) surface, followed by 4 L NO.

CO/Pd(111)

RAIR spectra for CO on Pd(111) at 320 K are plotted in Figure 2(a). CO exposure is measured in Langmuir and can only be related to coverage after further analysis. At 0.5 L exposure a peak at 1817 cm^{-1} is observed. This vibrational wavenumber agrees well with the observation of a peak at 1823 cm^{-1} in a previous RAIRS study[24] and is assigned to CO adsorbed in a three-fold hollow site. A weaker peak at 1900 cm^{-1} is also observed, which is assigned to CO bound to defect sites.[24] With increasing coverage both peaks shift to higher wavenumber as a result of dipole coupling, until at 10 L a dominant C-O stretching feature is observed at 1927 cm^{-1}. Looking in more detail at the changes with increasing exposure, it is seen that following 2 L exposure the low wavenumber CO vibrational band moves to 1828 cm^{-1}. By comparison with the literature, this exposure is assigned to a $\left(\sqrt{3}\times\sqrt{3}\right)R30°$ LEED structure, with a coverage of θ = 0.33 ML, which gives rise to a similar band at 1836 cm^{-1}.[24] Previous studies have shown that between θ = 0.33 and 0.5 ML, adsorbed CO occupies bridge and three-fold hollow sites, corresponding to the extremely broad bands observed at 3 - 5 L exposures. Previous work has also shown that above 0.5 ML coverage, CO also begins to occupy atop sites, which have stretching bands around 2075 cm^{-1}.[24-25] Weak bands at this wavenumber are observed at exposures of 5 L or above in Figure 2(a).

TPD experiments for different CO exposures are plotted in Figure 2(b) and confirm the relative coverage and point of saturation suggested by the RAIRS analysis, and are in agreement with previous studies.[26-27] Saturation was reached for exposures of 10 L with previous data showing that the room temperature saturation coverage is 0.6 ML.[24] Exposures of 2 L provide desorption yields of 60% of those for the saturated surface (Figure 2b), suggesting a coverage of 0.36 ML and confirming the assignments of the RAIR spectra. The TPD peak observed at 530 K gives an approximate first order desorption energy of between 147 – 167 kJ mol^{-1}, using the Redhead equation and assuming a value for the 1st order pre-exponential factor of between 10^{13} and 10^{15} s^{-1}.

NO/Pd(111)

RAIR spectra for NO on Pd(111) at 320 K are plotted in Figure 3a. At 0.5 L, one main vibrational band split into components at 1518 and 1550 cm^{-1} is observed. These bands are assigned to the stretching frequency of NO adsorbed in a three-fold hollow site. It is likely that the two bands arise due to slightly different environments. This assignment is in agreement with the only previous RAIRS room temperature study of NO/Pd(111).[28] At 10 L exposure, the higher wavenumber band grows to dominate and shifts to 1572 cm^{-1} as a result of dipole coupling. A smaller feature at 1816 cm^{-1} is also observed at 0.5 L, which increases in intensity until 1 L and then decreases until it disappears at 3 L exposure. This band is attributed to background CO adsorbed on three-fold sites during the cooling of the sample from the annealing temperature (1100-1200 K) to 320 K. The CO is gradually displaced by NO at higher NO exposures, resulting in the negative peak observed at $\geq$ 4 L. This assignment is based on scanning tunnelling microscopy (STM) and density functional theory (DFT) studies[25] as well as our own TPD and RAIRS studies of coadsorbed CO and NO (see below). Another band at 1652 cm^{-1} can be assigned either to NO adsorbed on bridge sites, as postulated by DFT calculations[29], or to NO adsorbed on defect sites.[20] A band of a similar frequency was observed in experiments for CO and NO coadsorbed on Pd(111), which Xu *et al.* attributed to NO adsorbed on bridge sites.[20] Xu *et al.* also studied CO and NO coadsorbed on Pd(100) where the NO band appeared around 1652 cm^{-1}. In Figure 3(a), the band at 1652 cm^{-1} is observed to increase in intensity even after CO is replaced by NO, hence we believe that this band is most likely to arise from NO adsorbed on (100) steps,[20] which are present as defects on our Pd(111) surface.

Previous TPD measurements of NO adsorbed on Pd(111) have indicated that NO dissociation is negligible.[28] However, in our TPD measurements (Figure 3b), the presence of

CO contamination at low coverages, and also the observation of adsorption on defect sites, complicates the TPD process. In addition to the NO peak (mass 30) we also observe small, but significant, desorption peaks at mass 28 (assigned as N_2 at high exposure ($\geq 4\ L$) but with a CO component at low exposure ($\leq 2\ L$) based on the TPD profiles and desorption temperature) and mass 44 (assigned as N_2O at high exposure ($\geq 4\ L$) but with a possible CO_2 component at low exposure ($\leq 2\ L$) based on the TPD profiles and desorption temperature). Note that it is not clear whether the high temperature N_2 peak observed arises directly from N_2 production, or whether it is a cracking fragment of N_2O in the mass spectrometer. Regardless of the source of the N_2, the observation of N_2O and N_2 indicates that the dissociation of NO occurs on the Pd(111) surface. Quantifying the contributions from the different processes is complicated by mass spectrometer sensitivity and pumping speed considerations, but it is clear from our measurements that as the NO exposure levels are increased, the integrated areas under the mass 28 (N_2/CO) and mass 44 (N_2O/CO_2) peaks are reduced slightly. The fraction of NO that is dissociated is therefore higher for lower NO exposures.

The TPD curve for NO (Figure 3(b)) shows a single desorption peak at 560 K, corresponding to NO adsorbed in a three-fold hollow site. Redhead analysis of the desorption temperature gives a desorption energy between 155-177 kJ mol^{-1}, assuming a value for the 1st order pre-exponential factor of between 10^{13} and 10^{15} s^{-1}.

Areas under the TPD curves were used, as with CO, to obtain a measure of coverage. Like CO, saturation coverage was achieved by 10 L exposure with the NO on Pd(111) saturation coverage being 0.5 ML.[28]

NO/CO/Pd(111)

Surfaces initially exposed to 2 L of CO are characterised using RAIRS and TPD following exposure to 0-10 L NO. RAIR spectra are plotted in Figure 4(a) and clearly show the effect of NO on the adsorbed CO. By comparison with Figures 2 and 3, and with the literature, we are able to assign the peaks. The RAIR spectrum resulting from the initial 2 L CO exposure is as already described in Figure 2. With increasing NO exposure the CO band observed at 1838 cm^{-1} initially broadens and then shifts to higher wavenumber (1892 cm^{-1}) due to the displacement of CO by NO from three-fold hollow sites to the less favourable bridge site.[30] With increasing NO exposure to > 4 L, the CO band shifts to lower wavenumbers, with the integrated peak area (Figure 4(b)) decreasing until it disappears at ~8 L NO exposure. A

second, much weaker, CO band assigned to adsorption on atop sites, based on previous RAIRS and LEED studies,[31] appears at exposures ≥ 2 L NO at 2062 cm^{-1}. This band increases slightly in intensity between 4 L and 5 L, then decreases again until it has completely disappeared by 8 L NO exposure. The RAIRS data clearly show that CO is displaced by NO. NO initially forces CO to occupy the less favoured bridge and atop sites due to the higher adsorption energy of the NO. The RAIR spectra also show two NO vibrational bands with increasing NO exposure. The main vibrational band at 1541-1574 cm^{-1} is assigned to NO adsorbed in a three-fold hollow site, while the band at 1651 cm^{-1} is assigned to NO adsorbed in defect sites.[20] RAIR spectra for 10 L NO on the surface initially dosed with 2 L CO are essentially the same as RAIR spectra for 10 L of NO on clean Pd(111) with two bands observed at 1572 and 1652 cm^{-1} in both cases, thus confirming that the pre-adsorbed CO has little effect on the NO RAIR spectrum. This is not surprising since the NO is seen to displace the CO.

Further evidence for the displacement of CO by NO is shown by plotting the integrated RAIR absorbance for CO (in the three-fold hollow and bridge sites) and NO (in the three-fold hollow site) for 2 L CO/Pd(111) as a function of increasing NO exposure in Figure 4(b). The figure clearly shows the CO peak area gradually decreasing, while the area under the peak for adsorbed NO increases at the same time. It also shows that there is almost no change in the integrated area under the three-fold hollow CO peak until 2 L NO is dosed onto the 2 L CO/Pd(111) surface and that the area under the CO or NO peak is not a linear function of NO exposure.

TPD has also been used to obtain information about the amount of CO and NO on the surface and about any thermal surface reactions that may be occurring. Figure 5 shows a comparison of TPD spectra of the co-adsorbed 4 L ^{15}NO/2 L CO/Pd(111) and 2 L ^{15}NO/2 L CO/Pd(111) and the pure systems, for CO and NO desorption as well as for the potential chemical products $^{15}N_2$ (mass 30), CO_2 (mass 44) and $^{15}N_2O$ (mass 46). The NO and CO TPD spectra are plotted after the application of an experimentally derived scaling factor which corrects for the detection efficiencies of the different isotopes of CO and NO in the mass spectrometer. The peak heights and areas under CO and NO the curves can therefore be compared directly for the data in Figure 5.

Despite the fact that the RAIR spectra for NO adsorbed on 2 L preadsorbed CO are effectively identical to those for pure NO, there are clearly some differences in the TPD spectra for NO in the presence of preadsorbed CO. The area under the TPD curves for 2 L

pure NO and 2 L ^{15}NO/2 L CO are essentially the same. However, the area of the NO peak for 4 L ^{15}NO/ 2 L CO is slightly larger compared to 4 L pure NO, suggesting that the preadsorbed CO enhances the NO uptake or, more likely, leads to less NO dissociation and hence more desorption of intact NO. Comparison of the 1652 and 1574 cm^{-1} peak heights in the NO RAIR spectra in Figures 3 and 4 confirms this. The spectra in Figure 4 shows smaller amounts of NO on defect sites (1652 cm^{-1} peak) where the occurrence of dissociation would be expected for NO adsorbed on top of preadsorbed CO, compared to pure NO. The pre-adsorbed CO hence blocks NO dissociation and leads to the desorption of more intact molecular NO. It is not possible to confirm this observation by comparing TPD peak areas for the desorption of N_2 and N_2O (which result from NO dissociation) for pure NO and ^{15}NO/2 L CO due to the different mass spectrometer sensitivities for mass 28 (Figure 3, N_2) and mass 30 (Figure 5, $^{15}N_2$), which it was not possible to quantify.

The TPD spectra for CO desorption from the ^{15}NO/2 L CO coadsorbed system clearly show the CO displacement by NO, also seen in RAIRS. The area under the CO TPD peak for the 2 L ^{15}NO/2 L CO and the 4 L ^{15}NO/2 L CO systems is much reduced compared to that for pure ^{13}CO. As well as a reduction in the CO TPD peak area, there is also a considerable shift in the peak shape and position, resulting in the appearance of two CO peaks in the 4 L ^{15}NO/2 L CO TPD trace. Whilst it is not clear exactly what is the cause of this, RAIRS shows that NO displaces CO and causes it to move to less favourable adsorption sites. The altered TPD profile and decreased peak temperature for CO in the presence of increasing amounts of NO is entirely consistent with this observation. The desorption peak with a maximum at 490 K is hence assigned to CO adsorbed in the bridge sites, while the desorption peak with a maximum at 552 K is assigned to CO adsorbed in the more favourable three-fold hollow sites. These assignments are based on the previously described RAIR spectra (Figure 4(a)) which indicate that with increasing NO exposure, CO is first moved from the three-fold hollow sites to the bridge and atop sites, before desorbing completely. The position of the peak maximum for CO shifts to a lower temperature for higher exposures of NO adsorbed on 2 L CO/Pd(111). Using the Redhead equation,[32] desorption activation energies for CO and NO can be estimated assuming first order desorption using a pre-exponential factor that can range between 10^{13} – 10^{15} s^{-1}. For 2 L ^{13}CO and 2 L ^{15}NO/ 2 L CO/ Pd(111) the CO peak maximum shifts from 530 K to 514 K, giving activation energies for first-order desorption between 147-167 kJ mol^{-1}, and 142-161 kJ mol^{-1} respectively. Increasing the NO exposure to 4 L ^{15}NO/ 2 L CO/ Pd(111) leads to a splitting of the peak, with two peaks observed at 490 K and 552 K giving desorption energies of between 135-153 kJ mol^{-1} (assigned to desorption

from bridge sites) and 152-174 kJ mol^{-1} (assigned to desorption from the three-fold hollow site). It should be noted that the population is primarily in the bridge sites by this point and the peak associated with the three-fold hollow sites is significantly lower in terms of its total area. Similarly, for the desorption of NO from the mixed systems we observe a shift in peak maximum from 575 K to 560 K with increasing NO exposure from 2 L ^{15}NO/ 2 L CO/Pd(111) to 4 L ^{15}NO/ 2 L CO/Pd(111). This corresponds to a change in desorption energy from 159-181 kJ mol^{-1} to 155-177 kJ mol^{-1} which matches the desorption energy of the pure 2 L NO/Pd(111) and 4 L NO/Pd(111) systems respectively. Clearly, CO has a small, but significant, effect on NO while significant concentrations of CO remain on the surface.

The TPD experiments also showed products from chemical reactions on the surface, notably N_2O, CO_2 and N_2 (see Figure 5). Due to the character of the molecular orbital that is active in the adsorption of NO, both molecular and dissociated NO species are often observed on metal surfaces.[33] The low internal bond energy of NO (630 kJ mol^{-1})[34] when compared to CO (1076 kJ mol^{-1})[34] also facilitates this process. CO_2, N_2 and N_2O are therefore formed as a result of the dissociation of NO on the surface, predominantly occurring on defects. There is currently no agreement about the mechanism for the CO + NO reaction on Pd. However, in a series of papers[35–37] it has been assumed that the mechanism is similar to that proposed by Peden[38] and Permana[39] for Rh. A key step in the reaction mechanism is the dissociation of NO, a process that was also observed for pure NO adsorbed on Pd(111) described above. As already discussed, it is not possible to directly compare the amount of N_2, N_2O and CO_2 produced in TPD for pure and coadsorbed systems. However, it seems that the presence of CO blocks NO dissociation somewhat, although crucially for the CO + NO reaction on Pd it does not completely inhibit it.

Figure 5 shows that the amount of reaction products observed in the TPD depends on the amount of ^{15}NO adsorbed on top of CO. The amount of $^{15}N_2O$ (mass 46) remains relatively unchanged for 4 L ^{15}NO/2 L CO compared to 2 L ^{15}NO/2 L CO. In contrast, the amount of $^{15}N_2$ is larger following the adsorption of 2 L ^{15}NO/2 L CO than for 4 L ^{15}NO/2 L CO. This was also observed for the pure system, where the amount of N_2 formed is higher for 2 L NO than for 4 L and 10 L NO exposures. For 2 L ^{15}NO/2 L CO, two $^{15}N_2$ peaks at ~ 550 K and 625 K are seen in the TPD spectrum. For 4 L ^{15}NO/2 L CO, the main peak observed is the lower temperature of these two peaks. Note that since N_2 is a cracking fragment of N_2O in the mass spectrometer, it is likely that the lower temperature $^{15}N_2$ peak, which is coincident with $^{15}N_2O$ desorption, is due to cracking of $^{15}N_2O$ in the mass spectrometer. The higher temperature peak however is directly assigned to the desorption of

$^{15}N_2$. Note that this peak was not observed for pure NO on Pd(111) (Figure 3), suggesting that a different mechanism occurs as a result of coadsorption. The reactions that occur as a result of NO dissociation are shown below:

$$NO_a \rightarrow N_a + O_a \quad (1)$$

$$N_a + N_a \rightarrow N_{2(g)} \quad (2)$$

$$N_a + NO_a \rightarrow N_2O_{(g)} \quad (3)$$

Figure 5 shows clear evidence for reaction (2) when NO and CO are coadsorbed. When pure NO is present on Pd(111) however, it is not clear whether the observed N_2 is from reaction (2) or from the cracking of N_2O, produced by reaction (3). Clearly NO dissociation occurs more readily for smaller amounts of NO on the surfaces, as for pure NO on Pd(111).

The TPD curves for CO_2 (mass 44) in Figure 5 also show larger amounts of CO_2 production for 2 L ^{15}NO/2 L CO compared to 4 L ^{15}NO/2 L CO. This is assigned to larger amounts of NO dissociation at lower exposures, but also to the presence of increased amounts of CO, which reacts with adsorbed O atoms to give CO_2. As the NO exposure increases, CO is displaced and hence less CO_2 is formed.

CO/NO/Pd(111)

Figure 6a shows RAIR spectra resulting from an initial 2 L dose of NO and subsequent exposure to CO. For 2 L NO exposure, three vibrational bands can be observed. The split band at 1549 and 1562 cm^{-1} is assigned to NO in three-fold hollow sites and the small band at 1651 cm^{-1} is assigned to NO adsorbed on defects. The band at 1822 cm^{-1} is assigned to the small amount of residual CO adsorbed in the three-fold hollow site from the background in the chamber, as described above. With increasing exposure of CO, the intensity of the band associated with NO in the three-fold hollow site decreases slightly and shifts to higher wavenumbers, while the band due to CO in the three-fold hollow site increases in intensity and shifts from 1822 to 1900 cm^{-1}. Figure 6b shows the integrated RAIR absorbance for CO (in the three-fold hollow and bridge sites) and NO (in the three-fold hollow site) for 2 L NO/Pd(111) as a function of increasing CO exposure. The total CO integrated area for the 10 L CO/2 L NO/Pd(111) system is lower than that for the pure 2 L CO on Pd(111) system (Figure 2). It is also noted that the integrated area under the NO peak is almost halved when the surface is subsequently exposed to 10 L CO and approximately matches the area of the 2

L NO/2 L CO/Pd(111) surface. The reduction in the NO integrated area suggests that CO can displace NO, but this is a much less likely process than NO displacing CO.

To further investigate the effect of CO on pre-adsorbed NO, TPD spectra for 4 L CO/2 L ^{15}NO/Pd(111) and 2 L CO/2 L ^{15}NO/Pd(111) are compared with the pure 2 L NO/Pd(111), 2 L CO/Pd(111) and 4 L CO/Pd(111) systems (Figure 7). As before, the CO and NO TPD spectra have been corrected for the mass spectrometer sensitivities for the different isotopes to allow direct comparisons. The TPD data in Figure 7 show that the amount of molecular NO desorption for both mixed systems is slightly higher than for the pure 2 L NO/Pd(111) system, as observed for the reverse coadsorbed system in Figure 5. As for the data shown in Figure 5, it is likely that this is due to reduced NO dissociation, and hence increased molecular NO desorption, for the coadsorbed system although the observed changes are relatively small. In contrast, the CO coverage is considerably reduced when compared with direct dosing of CO on a clean Pd(111) surface. The amount of CO adsorbed on the surface for 4 L CO/2 L ^{15}NO/Pd(111) is only slightly higher than the amount of CO for 2 L CO/2 L ^{15}NO/Pd(111) and both are significantly lower than the coverage when a clean surface is dosed with 4 L or 2 L CO. This occurs because of the higher binding energy of the NO, and is in agreement with the observations for NO adsorbed on top of CO (Figure 5). The profile of the CO TPD peak is also considerably changed when it is adsorbed on top of NO, compared to that of pure CO. In fact, the CO TPD curves in Figure 7 look similar to the low temperature CO TPD peak in Figure 5, suggesting that CO adsorbs on the less favourable bridge site as already discussed.

Combined with the changes in TPD peak area for CO there are also some changes in peak position. Using the Redhead equation, the activation energy for first order desorption can be estimated, using a value of the pre-exponential factor between 10^{13} - 10^{15} s^{-1}. For CO/^{13}CO the activation energy is between 146-167 kJ mol^{-1} for both pure systems, 4 L ^{13}CO/Pd(111) and 2 L ^{13}CO/Pd(111), and 140-159 kJ mol^{-1} for both mixed systems, 2 L CO/ 2 L ^{15}NO/Pd(111) and 4 L CO/ 2 L ^{15}NO/Pd(111). For NO the activation energy for desorption of the pure system, 2 L NO/Pd(111), is 155-176 kJ mol^{-1} and 158-180 kJ mol^{-1} for the mixed systems, 4 L CO/ 2 L ^{15}NO/Pd(111) and 2 L CO/ 2 L ^{15}NO/Pd(111). Coadsorption has opposite effects on the two substituents, decreasing the desorption activation energy of CO and increasing the desorption activation energy of NO, no matter what the sequence of dosing.

As before, we also monitored a number of chemical products (N_2, N_2O, and CO_2) following the coadsorption of CO and NO. Similar amounts of $^{15}N_2$, $^{15}N_2O$ and CO_2 are

produced for the 2 L CO/2 L ^{15}NO and 4 L CO/2 L ^{15}NO systems, which is unsurprising since all of these arise as a result of NO dissociation. Since the amount of NO changes little for these two experiments (as shown by both TPD and RAIRS) then this is as expected. The assignments of the two $^{15}N_2$ peaks is as for the NO/CO system where the lower temperature peak is assigned to cracking of $^{15}N_2O$ and the higher temperature peak is assigned to direct production of $^{15}N_2$. In addition, calculations show that the relative ratios of the integrated TPD areas for N_2, N_2O, and $^{13}CO_2$ to NO for both of the mixed systems is the same. Hence both mixed systems show a similar reaction mechanism for N_2 and N_2O formation, as may be expected due to the similar [NOa]/[COa] ratios of both systems. The TPD and RAIRS experiments therefore show that CO will displace pre-dosed NO to a small extent, but will not cause significant desorption.

3.2 Laser induced desorption

Having characterised the surface at a number of surface exposures, a series of fs-LID experiments were performed on both the pure and mixed systems. The resulting data was fitted to a power function (Equation 1), with a comparison of the retrieved *b* values discussed in terms of the different exposures and overlayer structures.

Individually Adsorbed CO and NO

The fs-LID yield is plotted as a function of laser fluence for CO on Pd(111) in Figure 8a for exposures of 2, 4 and 10 L. The points in the plot are the results of experimental measurements and the solid lines are least squares fits of Equation (1) to the data. The *b* parameters obtained from the fits (Table 1) are very similar: 3.4, 3.7 and 3.7 for 10, 4 and 2 L CO respectively, suggesting little difference in the LID of the CO as a function of coverage. At first sight this is surprising, since RAIRS data for CO (Figure 2) show changes in the CO overlayer structure with increasing exposure, which might be expected to affect the observed LID. However, assignments discussed earlier show that the CO molecule occupies the three-fold site over all exposure ranges with only a small amount of CO occupying the less favourable bridge site. Furthermore, the TPD data in Figure 2 show little change in the desorption of CO with increasing exposure. Since the *b* value is affected by desorption energy, this observation is therefore consistent with the TPD data seen in Figure 2.

The fs-LID yield is plotted as a function of fluence for NO on Pd(111) in Figure 8b for NO exposures of 2, 4 and 10 L. The energy range used is the same as in the CO experiments, although from the appearance of the curves alone it is clear that the behaviour is

significantly different. For higher exposures, we observe a clear deviation from the power law curve, with saturation of the first shot yield occurring well before the maximum fluence is reached, suggesting that the cross-section for laser induced desorption of NO is much larger than that for CO. The saturation of a first shot yield curve has been observed before in the highly efficient recombinative desorption of hydrogen on Ru(0001),[17] but to the best of our knowledge has not been previously observed for NO desorption.

The observation that NO desorbs more easily than CO is not related to the relative binding energies of the two molecules on the surface, since NO is more strongly bound than CO. This observation therefore suggests that NO is more photoactive than CO, with laser excitation leading to a greater probability of desorption for NO than CO. The exact reason for this is unclear, however the amphoteric bonding nature of NO, which allows NO to either donate its $2\pi^*$ (antibonding) electron to the surface or to accept electron density from the surface, could lead to a difference in the photo-activity of the two molecules. In addition, the small amount of dissociated N and O atoms found on the surface for NO adsorption, as already described, could also cause repulsions which would change the nature of the NO photo-activity compared to that of CO.

TABLE 1: Results of power law fits to the fs-LID data for pure CO(NO) exposure and for coadsorption of CO/NO and NO/CO on Pd(111).

	b	
Exposure	CO	NO
10 L CO(NO)/ Pd(111)	3.4 ± 0.1	5.0 ± 0.1
4 L CO(NO) / Pd(111)	3.7 ± 0.2	4.9 ± 0.2
2 L CO(NO) / Pd(111)	3.7 ± 0.1	3.4 ± 0.2
4 L CO/ 2 L NO/ Pd(111)	3.1 ± 0.3	2.9 ± 0.4
2 L CO/ 2 L NO/ Pd(111)	2.7 ± 0.2	3.9 ± 0.3
4 L NO/ 2 L CO/ Pd(111)	1.7 ± 0.5	3.4 ± 0.3
2 L NO/ 2 L CO/ Pd(111)	2.7 ± 0.4	2.6 ± 0.2

To provide a comparison of the NO data with that for CO, a subset of the NO yield versus fluence data is fitted to a power law curve to provide values for the exponent power *b*. The point at which to cut the data was chosen by initially fitting an s-logistic curve (Figure 8b) to the data plotted as a function of the average laser fluence. This provides a point of inflection above which artefacts arising from the roll-off prior to saturation would be observed. The subset of the data below the point of inflection is then fit to Equation 1, plotted in Figure 8c, with the retrieved *b* exponents given in Table 1.

Once the *b* parameter for the desorption process is characterised, yield-weighted fluence values can be calculated for the entire data set, allowing us to characterise the saturation fluence (f_{sat}). s-logistic curves are fitted to the entire data set plotted as a function of yield-weighted fluence (Figure 8b) for the 4 L and 10 L NO data providing f_{sat} values of 235 J m^{-2} and 180 J m^{-2} respectively. A good fit to the 2 L data could not be obtained due to the limited number of points at and above the saturation fluence. However, it is clear that the value is likely to be higher than that obtained for the higher coverages. The trend in saturation fluence therefore matches what would be expected from consideration of the changes in NO binding energy with increasing coverage. Previous TPD studies have demonstrated a strong binding energy dependence on the sample coverage for NO on Pd surfaces.[40] Energy barriers to desorption are seen to reduce from 180 kJ mol^{-1} for coverages around 0.03 ML to 90 kJ mol^{-1} at 0.34 ML.[40] The big decrease in desorption activation energy suggests there is a strong repulsion between the NO molecules on the surface, which reduces the desorption energy with increasing coverage. The repulsion between the NO molecules will also lead to a change in the electronic structure of the NO, thus changing its photoactivity. This is therefore seen in the change in saturation fluence, which shows a decreasing value with increasing coverage.

The *b* parameters retrieved for 4 L and 10 L pure NO exposure are almost identical with values of 4.9 and 5.0 respectively. The *b* parameter has been previously related to the desorption energy, and hence to the overlayer structure.[16,41] This is entirely consistent with the TPD and RAIRS measurements, which show approximately the same coverage and the same overlayer structure for these exposures. As the exposure is reduced to 2 L there is a large change in *b* with a value of 3.4. This change is indicative of a change in overlayer structure. This is consistent with RAIRS data (Figure 3) which show NO in two different three-fold sites following a 2 L exposure, whereas one peak grows to dominate the spectrum at higher NO exposures.

The increase in exponent with increasing exposure initially suggests that the lower exposure is less strongly bound to the surface, contrary to the TPD work discussed above which showed a reduction in the desorption energy as the coverage increased and to the values of f_{sat} derived from the data in Figure 8b. However, we note that the observations are complicated by some of the factors already outlined above. The overlayer structure at 2 L NO exposure is known to contain some CO contamination (~5% from the TPD measurement described above), although at such a low level of CO the effect on the desorption energy should be negligible. The other striking feature of the TPD data at 2 L compared to the 4 L and 10 L data is the slightly higher amounts of mass 28 (N_2/CO) and mass 44 (N_2O/CO_2) products when compared to the NO peak, suggesting that the degree of dissociation is higher for lower coverages. Contamination of the surface with atomic N and O, and the molecular products that can be produced (N_2/N_2O), will affect the desorption but in a way that is difficult to quantify. We also note that the *b* exponent depends on electron and phonon coupling which is expected to change with the changing overlayer structure.

Calculations based on the two temperature model[21] show that these observed changes in the *b* exponent value can be simulated with either a change in desorption energy *or* a change in electron/phonon adsorbate coupling time. In reality, the true effect will be a combination of the two as coverage is known to affect the binding to the surface (TPD and RAIRS results) and as different sites are populated the vibrational coupling across the sites will also change. Quantifying the true effect would require a proper measure of the binding energy through calorimetry measurements[42] combined with 2 pulse correlation (PC) as a first approximation to determine the vibrational coupling. While 2 PC has been used to provide coupling times for various molecular adsorbate systems[16-17], generally only a single electron and single phonon coupling is derived. 2 PC therefore only provides an effective coupling time for the system, in essence providing an average coupling for all the sites populated. Within the limitations of the two temperature model and the experimental yield versus fluence measurements, it is possible to obtain upper limits on the change in desorption energy for different coverages if we assume that only the desorption energy of the system changes. In other words assuming that the electronic and phononic coupling times do not change with surface coverage, then the observed changes in the experimentally observed yield versus fluence curves can be matched to theoretical curves with changes in the desorption energy on the order of a few 10s of kJ mol^{-1}.

Co-adsorbed CO and NO

The fs-LID yield versus fluence curves for NO and CO for surfaces initially dosed with CO are shown in Figure 9 and for surfaces initially dosed with NO in Figure 10. The fs-LID curves of NO (Figures 9b and 10b) for surfaces initially dosed with CO or NO both show saturation points, as in the individually adsorbed case. The CO fs-LID curves (Figure 9a and 10a) show no such saturation effects. We therefore treat the curves as above and initially fit to an s-logistic curve to find the point of inflection in the NO data. The data points before this are then taken forward and fitted to Equation 1 to allow for a comparison with the pure systems. The results of all fits are given in Table 1. From the table it is clear that coadsorption has a significant effect on the photodesorption process and that the structure of the overlayer is also important in dictating the observed photodesorption.

For the surface initially exposed to 2 L CO (Figure 9), subsequent exposure to 2 L NO reduces the surface coverage of CO slightly (Figure 4), and the shift in the observed RAIRS peak shows that the binding is shifted to bridge sites which weakens the binding to the surface and reduces the *b* value from 3.7 to 2.7, identical to the equivalent system with the dosing order reversed. At this exposure the NO coverage is spread over both three-fold hollow sites and (100) steps as shown by RAIRS. The measured *b* value for NO is 2.6, which is lower than that for the pure NO system and for the comparable system with the NO exposure first, 2 L CO / 2 L NO /Pd(111), which has a *b* value of 3.9. As seen in the TPD data described earlier, preadsorbed CO causes very little difference in the observed coverage of NO at 2 L exposure and a slight enhancement of the NO TPD peak at 4 L when compared to the pure system. This was explained as being due to the reduced number of defect sites available for dissociation which could lead to an increase in molecular NO desorption yield. However, the extra NO coverage is unlikely to lead to a significant change in the desorption energy or *b* value. It is therefore not clear what causes this lower b value for the 2 L NO/ 2 L CO system, however, as already discussed, it is expected that co-adsorption leads to changes in the electronic structure of the adsorbate(s) hence leading to changes in the electron and phonon coupling, which would affect the measured *b* value..

Increasing the exposure of NO to 4 L reduces the coverage of CO dramatically, with a significant proportion of the CO molecules now in atop sites. The *b* value for CO is very low in this situation, at 1.7. However, it should be noted that at such low coverage the noise level in this data and the resulting quality of fit are much lower than for all other systems. While we can be confident that the *b* value is significantly lower, the absolute value has large errors associated with it. Conversely, the NO coverage has increased, with an increased population in both three-fold hollow and (100) step sites as shown earlier with RAIRS. With such a low

concentration of CO on the surface we now obtain an identical *b* value to that observed for pure NO, suggesting that the small CO coverage is having a negligible effect on the NO and that the system is now behaving as though the CO had not been dosed on to the surface at all. Clearly the observed changes in *b* values for the mixed systems reflect the observed changes in the overlayer structures, as determined by RAIRS and TPD.

Considering the system initially dosed with 2 L NO (Figure 10), RAIRS confirms that the molecules are in three-fold hollow sites. As the surface is subsequently exposed to 2 L CO a small amount of NO is displaced, leading to a reduced coverage of NO in three-fold hollow sites. The CO also adsorbs in three-fold hollow sites. Hence there is a competition between the two molecules for adsorption on the surface. As seen in Table 1, the mixture of species on the surface leads to a slight increase in the *b* value for NO when CO is adsorbed on top of 2 L NO (3.4 for pure NO compared with 3.9 for NO adsorbed on top of CO). This is initially somewhat surprising considering what looks to be a destabilising effect of the CO molecules on NO – the NO RAIRS peak decreases in intensity when CO is adsorbed on top (Figure 6) - which would be expected to lead to a reduction in *b*. However, it is not clear exactly what effect coadsorption will have on the electronic structure of the surface, and any changes will likely lead to changes in the LID. TPD data (Figure 7) do not show a large change in the desorption temperature of NO when CO is adsorbed on top. Hence it is more likely that the *b* value changes due to changes in the electronic structure of the surface and adsorbate which affects the electron and phonon coupling. The CO adsorbed on the surface is at a lower coverage than is seen from exposure of 2 L CO to a clean Pd(111) surface (see TPD, Figure 7) and has a derived *b* value of 2.7, which is much lower than that observed for 2 L CO/ Pd(111) system (3.7). This is entirely expected due to the strong reduction seen in the desorption energy of CO when it is dosed on to a surface initially exposed to NO (Figure 7).

As the exposure is increased to 4 L CO, the *b* value for NO is reduced to 2.9. The increased exposure of CO increases the CO coverage only very slightly; however, the limited ability of CO to displace NO from the Pd(111) surface means that some of the CO molecules adsorb on atop sites as well as the more favoured three-fold hollow sites. This means that the *b* value is increased to 3.1, closer to the pure CO value.

Reaction Products

Depletion curves for the reaction products (N_2, N_2O and CO_2) observed for the coadsorbed systems were also recorded for an average laser fluence of 24 mJ cm^{-2}. With these

experiments we were looking for differences in the thermal and photon driven reactivity of the system rather than effects due to the laser fluence dependence. The changes in first shot yields of all reaction products are presented in Table 2.

TABLE 2: fs-LID first shot yield values for the reaction products CO_2, N_2O and N_2 for the coadsorption systems.

	First shot yield/ counts s^{-1}			
	2 L NO/2 L CO	4 L NO/2 L CO	2 L CO/2 L NO	4 L CO/2 L NO
CO_2	-	8000	2900	12000
N_2O	-	300	-	-
N_2	-	4600	3100	2300

For the surfaces initially dosed with CO, N_2 laser induced desorption (Table 2) is seen to decrease by about 20-25% with increasing CO exposure. In contrast, for CO adsorbed on top of NO, the amount of N_2/N_2O produced in the TPD (thermal) process does not change with increasing CO exposure (Figure 7). However, for NO adsorbed on top of CO (Figure 5), larger amounts of N_2 are seen for lower NO exposures. As described above, this reduction in yield for both thermal and laser driven processes is most likely due to the saturation of the defect sites required to dissociate NO, as the NO coverage increases. For surfaces initially doped with CO(NO), thermal desorption of N_2O is unchanged with increasing exposure to NO(CO). In the fs-LID experiments, a quantifiable amount of N_2O is only seen for the 4 L NO/2 L CO/Pd(111), making a comparison of the relative changes in yield difficult.

For CO_2 there are clear differences between the thermal and laser driven desorption. For surfaces initially dosed with NO, there is a large increase in CO_2 laser induced desorption yield with increasing CO exposure (Table 2). This contrasts with an unchanged CO_2 thermal desorption yield for CO adsorbed on top of NO (figure 7). The thermal desorption yield for increasing amounts of NO adsorbed on top of CO (Figure 5) decreases with increasing NO exposure.

Based on these observations it is difficult to explain the dramatic changes with coverage. One would expect that the availability of atomic oxygen and the coverage of CO would be the most significant parameters when considering the yield of CO_2. For a thermally driven process it would be expected that the yield of CO_2 reduces with reduced CO coverage

and this is exactly as is observed in the TPD data for the 2 L NO/2 L CO/Pd(111) and 4 L NO/2 L CO/Pd(111), with a large drop in CO_2 production (Figure 5) associated with a reduction in CO coverage due to its displacement by NO. For the system where NO is adsorbed first however, there is no change in the amount of CO_2 produced with increasing NO exposure for the thermal process (Figure 7). In contrast, a much increased amount of CO_2 is produced with increasing CO exposure for the laser driven process. This suggests that the femtosecond laser irradiation may be efficient in inducing NO dissociation, compared to the thermal process. This therefore enhances the amount of CO_2 produced in the laser driven process. However, further experiments would be needed to conclusively confirm this observation.

4. Summary

We have employed RAIRS, TPD and fs-LID to characterise and probe the desorption of CO, NO and CO + NO on Pd(111) at a number of different coverages. Our RAIRS studies allow us to characterise the surfaces and are in good agreement with previous reported studies. Our RAIRS and TPD studies of the coadsorbed systems show that the NO can displace the CO and, importantly, that a range of different reaction products are produced as a result of the coadsorption including N_2, N_2O and CO_2. Whilst CO does not displace NO directly, data clearly show that the coadsorption of CO on top of NO also affects the NO. Our comparison of conventional TPD measurements and fs-LID allows us to gain additional insight into the desorption dynamics of CO, NO and CO + NO on Pd(111). We find that desorption of CO on Pd(111) follows a power law and is fairly independent of CO coverage, but for NO on Pd(111) we observe a clear deviation from a power law curve at higher coverages. This suggests that the cross-section for laser induced desorption of NO is much larger than that for CO and that NO on Pd(111) is more photoactive than CO on Pd(111). Interestingly, for CO + NO on Pd(111), we find that co-adsorption has a strong influence on the photodesorption process with different reaction products also being observed for the laser induced and thermally induced desorption.

Acknowledgements

This work was supported by the EPSRC through grant EP/D068673/1. RSM would like to thank UCL and the Ramsay trust for a research fellowship and the Royal Society for a University Research Fellowship (UF100047). We thank Peter Saalfrank for useful discussions. We also thank Daren Burke for assistance with some of the figures and for

critical reading of the manuscript.

References

1. J. Gladh, T. Hansson and H. Ostrom, *Surf. Sci.*, 2013, **615** 65.

2. T. Yamanaka, A. Hellman, S. W. Gao and W. Ho, *Surf. Sci.*, 2002, **514**, 404.

3. F. Budde, T. F. Heinz, A. Kalamarides, M. M. T. Loy and J. A. Misewich, *Surf. Sci.* 1993, **283**, 143.

4. F. Budde, T. F. Heinz, M. M. T. Loy, J. A. Misewich. F. Derougemont and H. Zacharias, *Phys. Rev. Lett.* 1991, **66**, 3024.

5. J. A. Prybyla, T. F. Heinz, J. A. Misewich, M. M. T. Loy and J. H. Glownia, *Phys. Rev. Lett.* 1990, **64**, 1537.

6. F. J. Kao, D. G. Busch, D. Cohen, D. G. Dacosta and W. Ho, *Phys. Rev. Lett.* 1993, **71**, 2094.

7. T. H. Her, R. J. Finlay, C. Wu and E. Mazur, *J. Chem. Phys.* 1998, **108**, 8595.

8. S. Deliwala, S. Frischkorn, M. Wolf, T. H. Her, W. D. Mieher and E. Mazur, *Chem. Phys. Lett.* 1995, **242**, 617.

9. J. A. Misewich, A. Kalamrides, T. F. Heinz, U. Hofer and M. M. T. Loy, *J. Chem. Phys.* 1994, **100**, 736.

10. J. A. Misewich, S. Nakabayashi, P. Weigand, M. Wolf and T. F. Heinz, *Surf. Sci.* 1996, **363**, 204.

11. L. M. Struck, L. J. Richter, S. A. Buntin *et al.*, *Phys. Rev. Lett.* 1996, **77**, 4576.

12. M. Bonn, S. Funk, C. Hess, D. N. Denzler, C. Stampfl, M. Scheffler, M. Wolf and G. Ertl, *Science*, 1999, **285**, 1042.

13. S. Funk, M. Bonn, D. M. Denzler, C. Hess, M. Wolf and G. Ertl, *J. Chem. Phys.* 2000, **112**, 9888.

14. J. A. Prybyla, H. W. K. Tom and G. D. Aumiller, *Phys. Rev. Lett.* 1992, **68**, 503.

15. E. H. G. Backus, A. Eichler, A. W. Klein and M. Bonn, *Science*, 2005, **310**, 1790.

16. P. Szymanski, A. L. Harris and N. Camillone, *J. Phys. Chem. A*, 2007, **111**, 12524.

17. D. N. Denzler, C. Frischkorn, M. Wolf and G. Ertl, *Journal of Physical Chemistry B*, 2004, **108**, 14503.

18. P. Nuernberger, D. Wolpert and G. Gerber, *PNAS*, 2010, **107** 10366.

19. P. Nuernberger, D. Wolpert, H. Weiss and G. Gerber, *Phys. Chem. Chem. Phys.* 2012, **14** 1185.

20. X. P. Xu, P. J. Chen and D. W. Goodman, *J. Phys. Chem.* 1994, **98**, 9242.

21. M. Brandbyge, P. Hedegard, T. F. Heinz, J. A. Misewich and D. M. Newns, *Phys. Rev. B*, 1995, **52**, 6042.

22. C. Frischkorn and M. Wolf, *Chem. Rev.*, 2006, **106**, 4207.
23. D. E. Gray, *American Institute of Physics Handbook* - 3rd ed. (McGraw-Hill, New York, 1972).
24. A. M. Bradshaw and H. M. Hoffman, *Surf. Sci.*, 1978, **72**, 513.
25. M. K. Rose, T. Mitsui, J. Dunphi, A. Borg, D. F. Ogletree, M. Salmeron and P. Sautet, *Surf. Sci.*, 2002, **512**, 48.
26. I. Stara and V. Matolin, *Surf. Sci.*, 1994, **313**, 99.
27. X. C. Guo and J. T. Yates, *J. Chem. Phys.* 1989, **90**, 6761.
28. I. Nakamura, T. Fujitani and H. Hamada, Surf. Sci., 2002, **514**, 409.
29. D. Loffreda, D. Simon and P. Sautet, *Chem. Phys. Lett.* 1998, **291**, 15.
30. K. Honkala, P. Pirila and K. Laasonen, *Surf. Sci.*, 2001, **489**, 72.
31. A. M. Bradshaw and F. M. Howmann, *Surf. Sci.*, 1978, **72**, 513.
32. P. A. Redhead, **12**, *Vacuum*, 203 (1962).
33. W. A. Brown and D. A. King, *J. Phys. Chem. B*, 2000 **104**, 11440.
34. *Handbook of Chemistry and Physics*. (CRC Press, 1973).
35. G. Prévot, and C. R. Henry, *J. Phys. Chem. B*, 2002, **106**, 12191.
36. K. Nakao, S. Ito, K. Tomishige and K. Kunimori, *J. Phys. Chem. B*, 2005, **109**, 17579.
37. K. Thirunavukkarasu, *K.* Thirumoorthy, J. Libuda and C. S. Gopinath, *Catal. Lett.* 2005, **109**, 13272.
38. C. H. F. Peden, D. N. Belton and S. J. Schmieg, *J. Catal.* 1995, **155**, 204.
39. H. Permana, K. J. Simon Ng, C. H. F. Peden, S. J. Scmieg, D. K. Lambert and D. N. Belton, *J. Catal.* 1996, **164**, 194.
40. R. D. Ramsier, Q. Gao, H. N. Waltenburg, K. W. Lee, O. W. Nooij, L. Lefferts and J. T. Yates, *Surf. Sci.* 1994, **320**, 209.
41. Szymanski, P.; Harris, A. L.; Camillone, N., III. *J. Chem. Phys.* 2007, **126**, 214709.
42. W.A. Brown, R. Kose and D.A. King, *Chem. Rev.* 1998, **98,** 797-831.

Figure Captions

Figure 1.

(a) Experimental layout showing the optical path and UHV chamber used for the fs-LID experiments. The laser beam is passed through a half waveplate (WP) and polarising beam splitter (PBS) to control the laser fluence. A telescope reduces the beam diameter to approximately 1 mm and is subsequently passed into the UHV chamber where it hits the Pd(111) surface. The beam can also be picked off before entering the UHV chamber to allow for the beam profile to be measured. (b) Experimental depletion curves for the LID of NO at 24 mJ cm^{-2}. The data is fitted to a bi-exponential curve (solid line) to retrieve the first shot desorption yield.

Figure 2

(a) RAIR spectra at 320 K for a series of exposures between 0 and 10 L for CO adsorbed on Pd(111) at room temperature. (b) TPD spectra for CO adsorbed on Pd(111) for 2 L, 4 L and 10 L CO exposure.

Figure 3

(a) RAIR spectra at 320 K for a series of exposures between 0 and 10 L for NO on Pd(111). (b) TPD spectra for NO on Pd(111) for 2 L, 4 L and 10 L exposure recorded for NO (mass 30), CO_2/N_2O (mass 44) and N_2/CO (mass 28) desorption products.

Figure 4

(a) RAIR spectra at 320 K for a series of exposures between 0 and 10 L NO adsorption on 2 L CO/Pd(111). (b) Integrated RAIR absorbance for CO (in the three-fold hollow and bridge sites) and NO (in the three-fold hollow site) for 2 L CO/Pd(111) as a function of increasing NO exposure.

Figure 5

TPD spectra of mass 28/29 (CO/^{13}CO), mass 30/31 (NO/^{15}NO), mass 30 ($^{15}N_2$), mass 46 ($^{15}N_2O$) and mass 44 (CO_2) following ^{15}NO adsorption on 2 L CO/Pd(111) at 320 K at 2 L and 4 L NO exposure. TPD curves for pure ^{13}CO and pure NO adsorption are included for comparison. The 2 L ^{13}CO TPD curve is multiplied by 1.6, and the 2 L NO and 4 L NO curves are divided by 1.8, to compensate for different mass spectrometer sensitivities of the different isotopes.

Figure 6

(a) RAIR spectra at 320 K for a series of exposures between 0 and 10 L CO adsorption on 2 L NO/Pd(111). (b) Integrated RAIR absorbance for CO (in the three-fold hollow and bridge sites) and NO (in the three-fold hollow site) for 2 L CO/Pd(111) as a function of increasing NO exposure.

Figure 7

TPD spectra of mass 28/29 ($CO/^{13}CO$), mass 30/31 ($NO/^{15}NO$), mass 30 ($^{15}N_2$), mass 46 ($^{15}N_2O$) and mass 44 (CO_2) following CO adsorption on 2 L ^{15}NO/Pd(111) at 320 K taken at 2 L and 4 L CO exposure. TPD curves for pure ^{13}CO and pure NO adsorption are included for comparison. The same sensitivity corrections are applied as in Figure 5 to allow direct comparison between pure and coadsorbed systems.

Figure 8

CO yield-*vs*-fluence dependence curves for adsorption at 340 K for pure CO/Pd(111) (a). NO yield-*vs*-fluence dependence curves at 340 K for pure NO/Pd(111) (b and c). Solid lines in a and c are power fits to the data, while the solid line in b is a sigmoid curve.

Figure 9

CO yield-*vs*-fluence dependence curves at 340 K for NO/CO/Pd(111) (a). NO yield-*vs*-fluence dependence curves at 340 K for NO/CO/Pd(111) (b and c). Solid lines in a and c are power fits to the data while the solid line in b is a sigmoid curve.

Figure 10

CO yield-*vs*-fluence dependence curves at 340 K for CO/NO/Pd(111) (a). NO yield-*vs*-fluence dependence curves at 340 K for CO/NO/Pd(111) (b and c). Solid lines in a and c are power fits to the data while the solid line in b is a sigmoid curve.

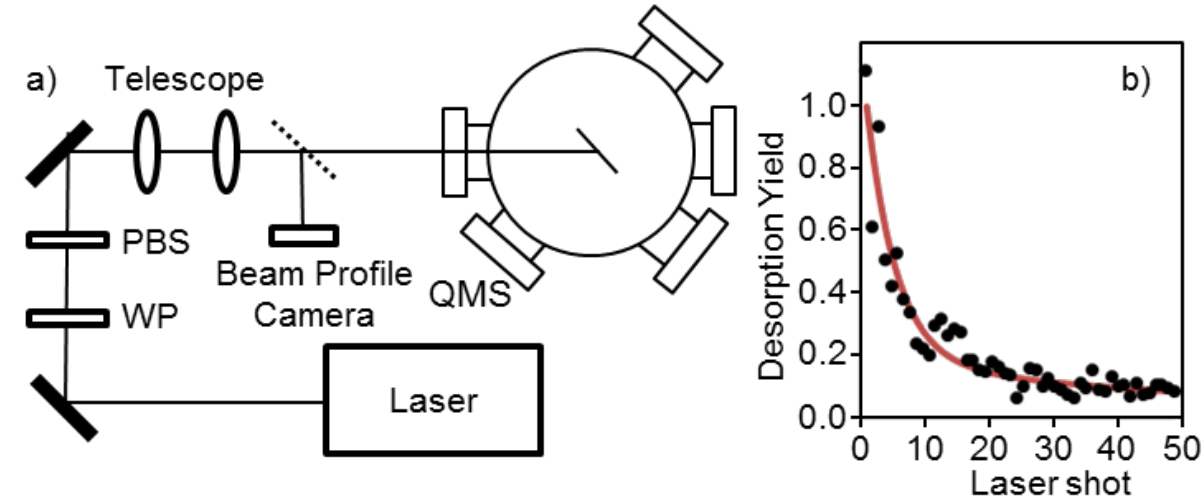
a)
Telescope
PBS
WP
Beam Profile
Camera
QMS
Laser
b)
Desorption Yield
1.0
0.8
0.6
0.4
0.2
0.0
0
10
20
30
40
50
Laser shot

Figure 1

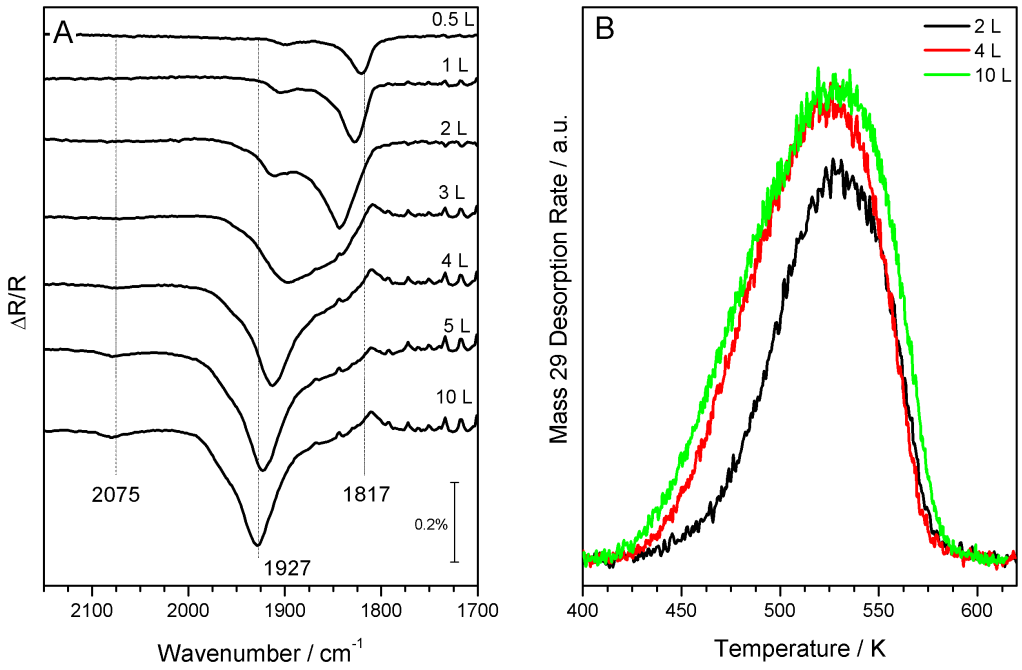
A
0.5 L
1 L
2 L
3 L
4 L
5 L
10 L
2075
1817
1927
0.2%
ΔR/R
2100
2000
1900
1800
1700
Wavenumber / cm-1
B
2 L
4 L
10 L
Mass 29 Desorption Rate / a.u.
400
450
500
550
600
Temperature / K

Figure 2

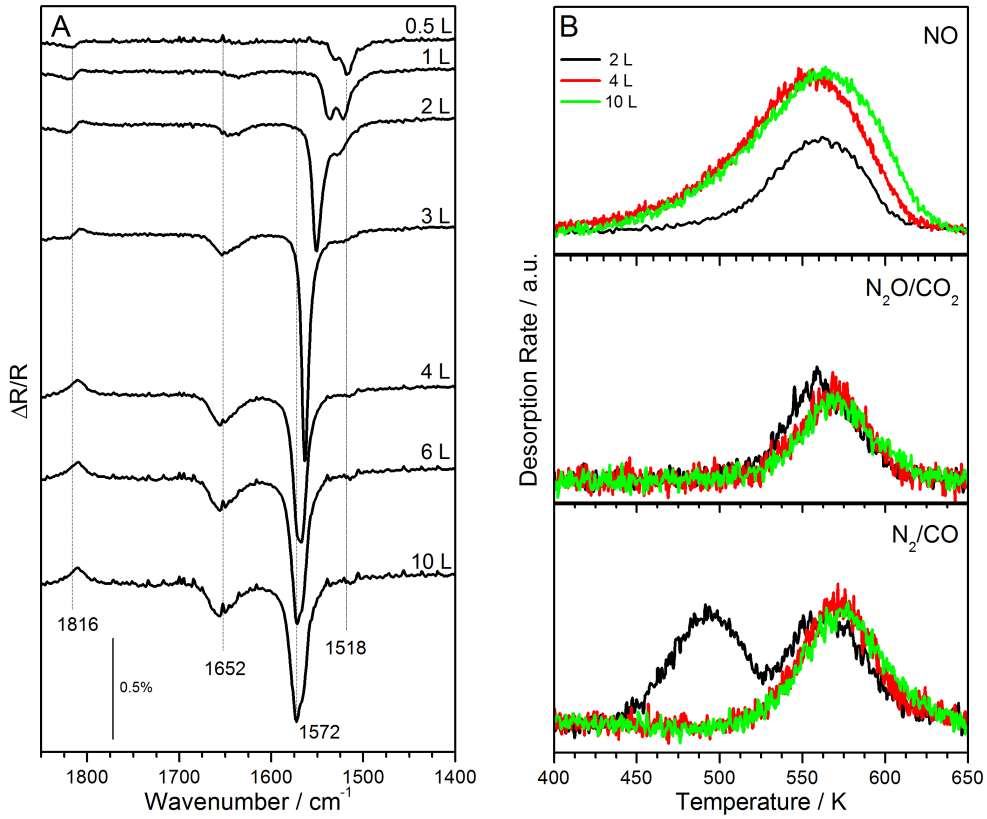
A
0.5 L
1 L
2 L
3 L
4 L
6 L
10 L
1816
1652
1572
1518
0.5%
ΔR/R
1800
1700
1600
1500
1400
Wavenumber / cm-1
B
NO
2 L
4 L
10 L
N2O/CO2
N2/CO
Desorption Rate / a.u.
400
450
500
550
600
650
Temperature / K

Figure 3

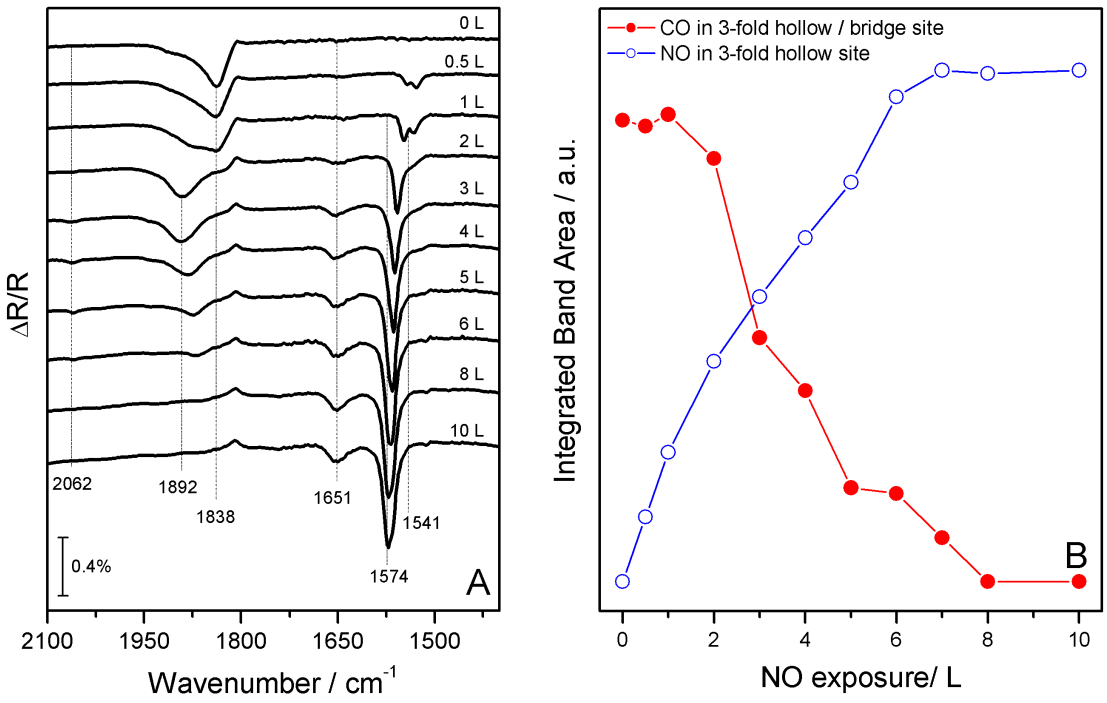
0 L
0.5 L
1 L
2 L
3 L
4 L
5 L
6 L
8 L
10 L
2062
1892
1838
1651
1574
1541
0.4%
A
ΔR/R
2100
1950
1800
1650
1500
Wavenumber / cm-1
CO in 3-fold hollow / bridge site
NO in 3-fold hollow site
Integrated Band Area / a.u.
B
0
2
4
6
8
10
NO exposure/ L

Figure 4

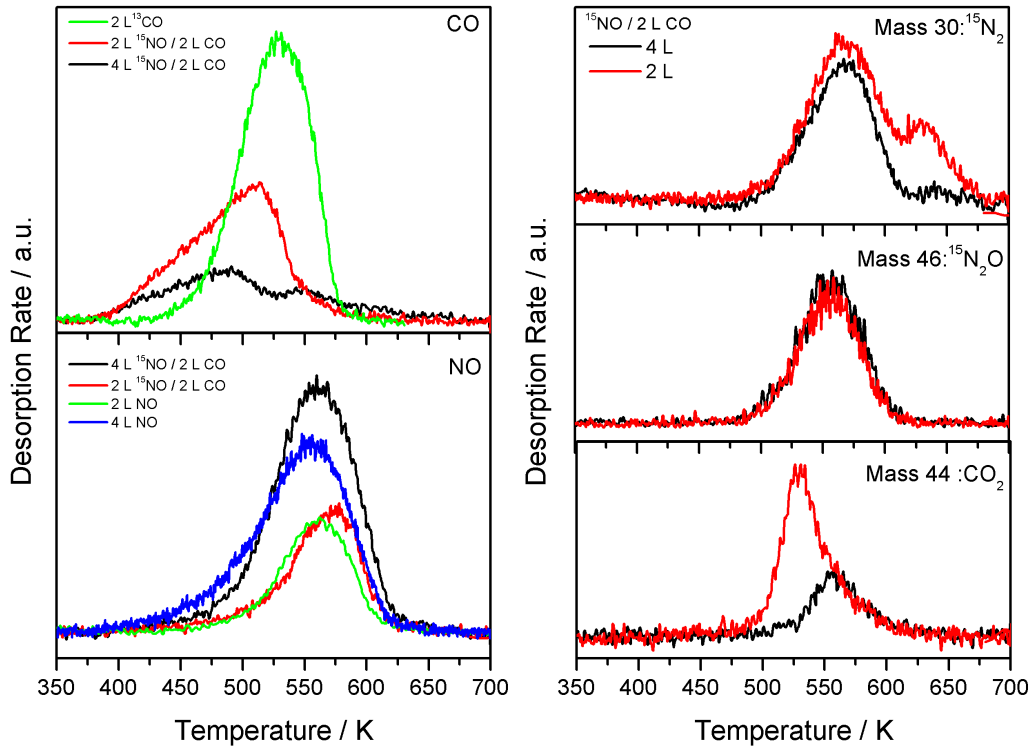
2 L ^{13}CO
2 L ^{15}NO / 2 L CO
4 L ^{15}NO / 2 L CO
CO
4 L ^{15}NO / 2 L CO
2 L ^{15}NO / 2 L CO
2 L NO
4 L NO
NO
Desorption Rate / a.u.
350 400 450 500 550 600 650 700
Temperature / K
^{15}NO / 2 L CO
4 L
2 L
Mass 30:^{15}N$_2$
Mass 46:^{15}N$_2$O
Mass 44 :CO$_2$
Desorption Rate / a.u.
350 400 450 500 550 600 650 700
Temperature / K

Figure 5

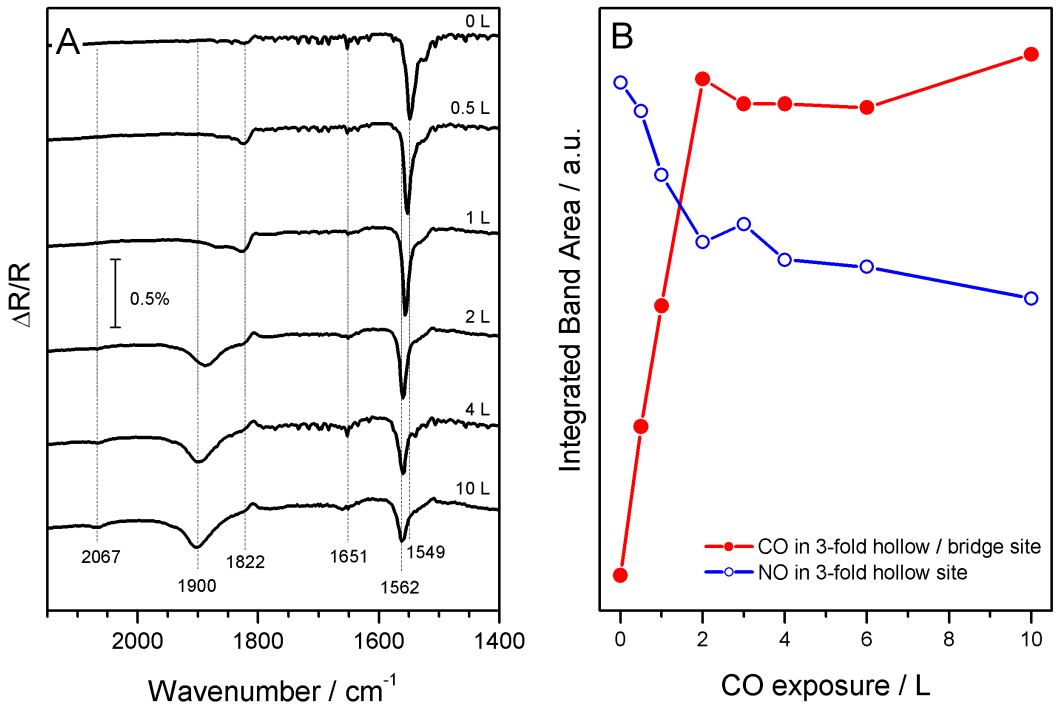
A
0 L
0.5 L
1 L
2 L
4 L
10 L
0.5%
ΔR/R
2067
1900
1822
1651
1562
1549
2000
1800
1600
1400
Wavenumber / cm-1
B
Integrated Band Area / a.u.
CO in 3-fold hollow / bridge site
NO in 3-fold hollow site
0
2
4
6
8
10
CO exposure / L

Figure 6

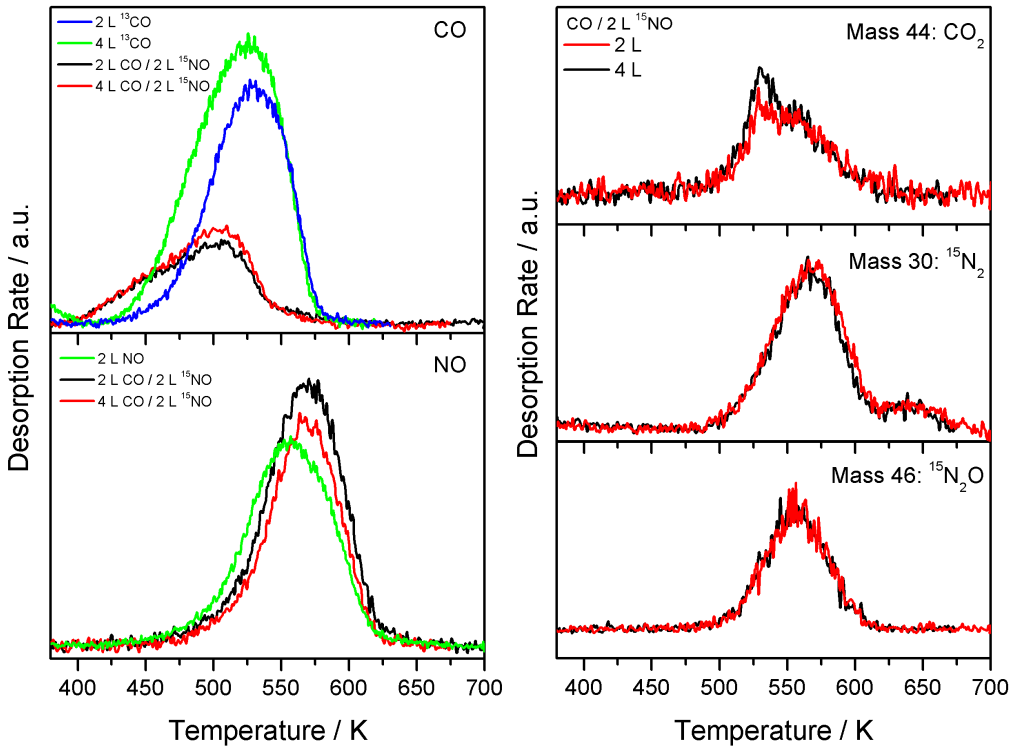
2 L 13CO
4 L 13CO
2 L CO / 2 L 15NO
4 L CO / 2 L 15NO
CO
2 L NO
2 L CO / 2 L 15NO
4 L CO / 2 L 15NO
NO
Desorption Rate / a.u.
400 450 500 550 600 650 700
Temperature / K
CO / 2 L 15NO
2 L
4 L
Mass 44: CO2
Mass 30: 15N2
Mass 46: 15N2O
Desorption Rate / a.u.
400 450 500 550 600 650 700
Temperature / K

Figure 7

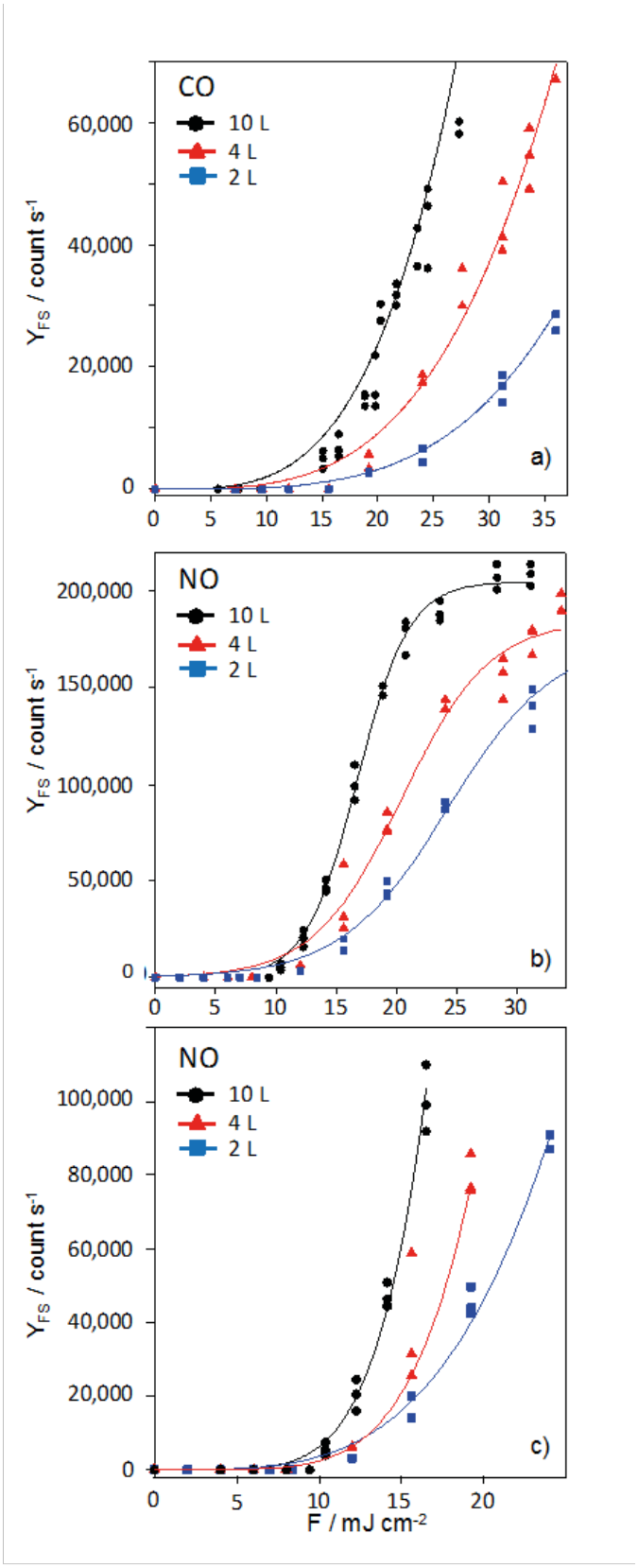
CO
10 L
4 L
2 L
Y_{FS} / count s^{-1}
60,000
40,000
20,000
0
0
5
10
15
20
25
30
35
a)
NO
10 L
4 L
2 L
Y_{FS} / count s^{-1}
200,000
150,000
100,000
50,000
0
0
5
10
15
20
25
30
b)
NO
10 L
4 L
2 L
Y_{FS} / count s^{-1}
100,000
80,000
60,000
40,000
20,000
0
0
5
10
15
20
F / mJ cm^{-2}
c)

Figure 8

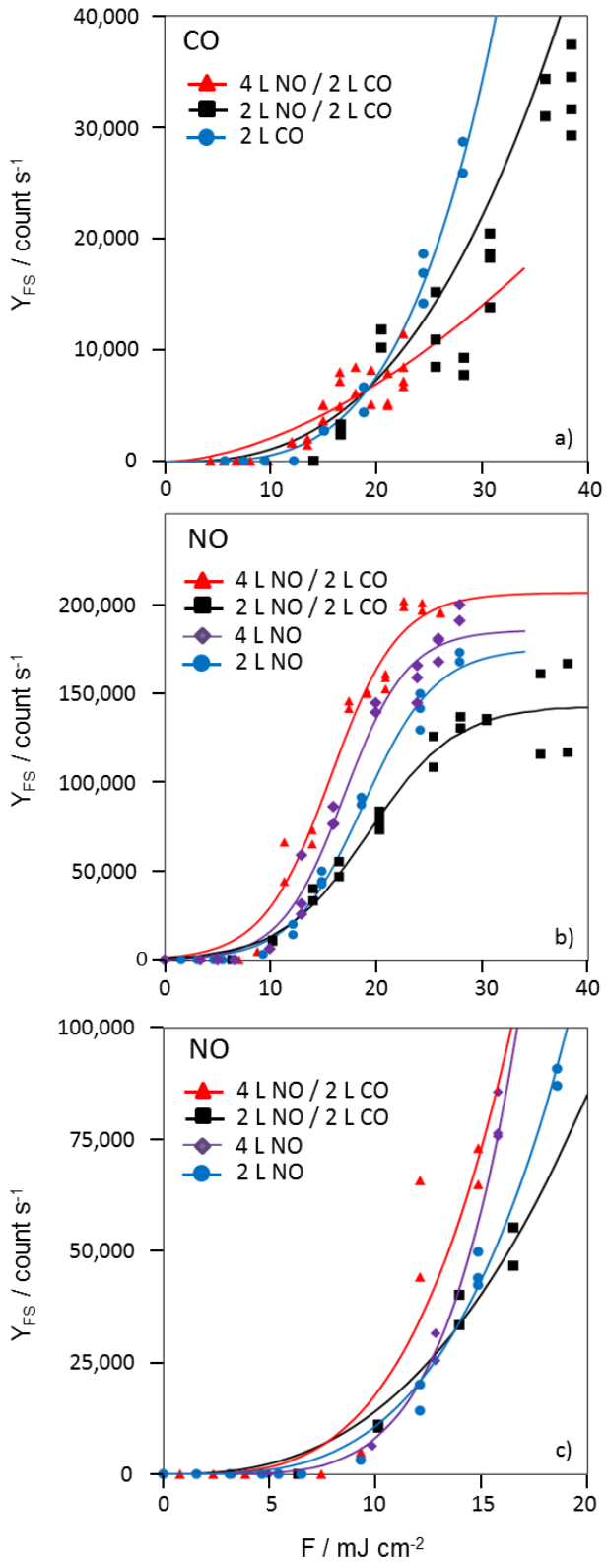
CO
4 L NO / 2 L CO
2 L NO / 2 L CO
2 L CO
a)
NO
4 L NO / 2 L CO
2 L NO / 2 L CO
4 L NO
2 L NO
b)
NO
4 L NO / 2 L CO
2 L NO / 2 L CO
4 L NO
2 L NO
c)
Y_FS / count s^-1
F / mJ cm^-2

Figure 9

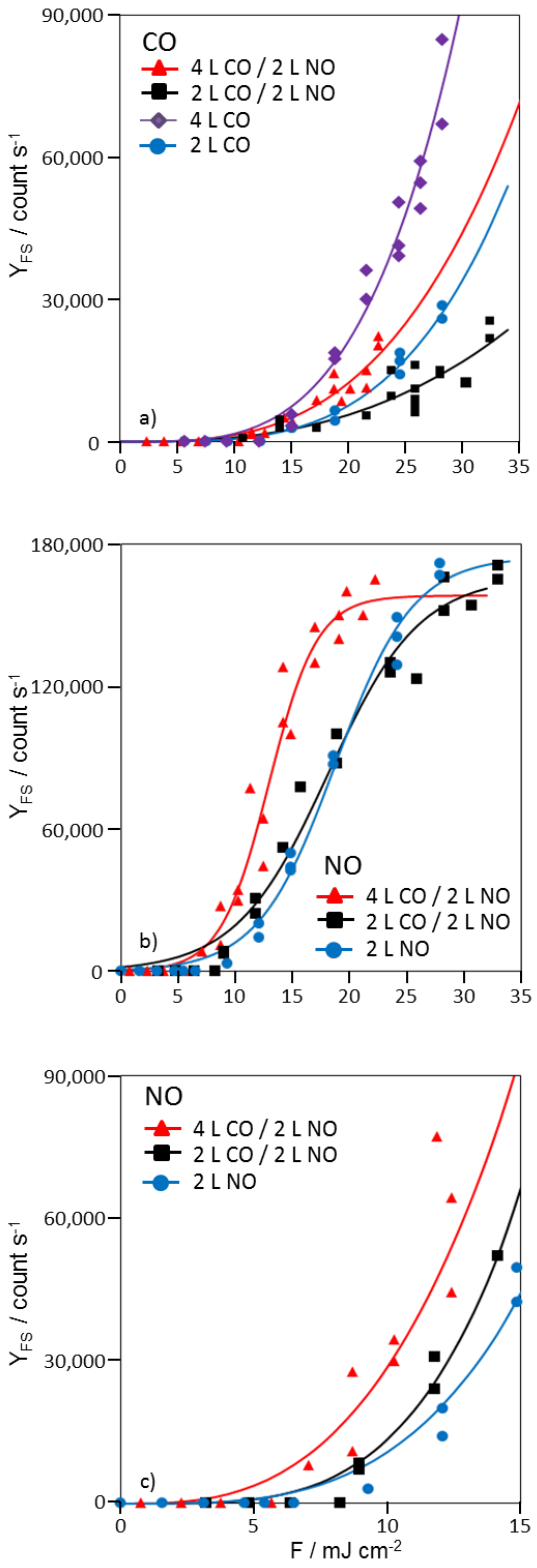
CO
4 L CO / 2 L NO
2 L CO / 2 L NO
4 L CO
2 L CO
a)
b)
NO
4 L CO / 2 L NO
2 L CO / 2 L NO
2 L NO
c)
NO
4 L CO / 2 L NO
2 L CO / 2 L NO
2 L NO
Y_FS / count s^-1
F / mJ cm^-2

Figure 10